Journal of Nano Research
ISSN: 1661-9897, Vol. 77, pp 87-104
doi:10.4028/p-82qxbi

Submitted: 2022-07-25
Revised: 2022-10-20
Accepted: 2022-10-21
Online: 2023-03-30

Effect of ZnO Nanoparticles Salt Precursors on Structural, Morphological, Optical and MB Photocatalytic Properties Using Hydrothermal Synthesis

Hicham BAHTOUN[1,a*], Lazhar HADJERIS[1,b], Sabrina IAICHE[2,c] and Tarek Ouniss DIAB[3,d]

[1] LMSSEF Laboratory of Materials and Structure of Electromechanical Systems and their Reliability (LMSSEF), Larbi Ben M'Hidi University, Oum El Bouaghi, 04000, Algeria.

[2]Laboratory of Structures, Proprieties and Inter Atomic Interactions (LASPI2A), Sciences Matter Department, Faculty of Science and Technology, University of Abbes Laghrour, Khenchela 40000, Algeria.

[3] Active Components and Materials Laboratory (LCAM), Université Larbi Ben M'Hidi, Oum El Bouaghi, 04000, Algeria.

[a]email: hichambahtoun2022@gmail.com, [b]email: lazhar.hadjeris@univ-oeb.dz, [c]email: sabrina.iaiche@univ-khenchela.dz, [d]email: otarekdiab@yahoo.fr

Keywords: Zinc acetate; Zinc nitrate; Zinc chloride; ZnO powder; Photocatalysis; Methylene blue; Crystallinity; Morphology.

Abstract. Zinc oxide ZnO nanoparticles were successfully produced via a simple low cost hydrothermal method using different metal precursors. Zinc acetate $Zn(CH_3COO)_2$, Zinc nitrate ($Zn(NO_3)_2$) and Zinc chloride ($ZnCl_2$) were the source materials. The obtained nanoparticles were investigated by means: X-ray diffraction (XRD), Scanning Electron Microscopy (SEM) and Differential Reflectance spectroscopy (DRS). The XRD exhibited the high crystallinity of the pure ZnO phase with hexagonal wurtzite crystalline structure for all simples excepted for ZnO synthetized from $ZnCl_2$ precursor. The crystallite sizes were estimated in the range of 20-37 nm. The precursor type does not affect the E_g of the nanoparticles. The bandgaps energies were between 3.21-3.22eV. The type of precursor affect the particles morphology. SEM images reveal different morphologies. The photocatalytic activity of the synthetized ZnO (zinc oxide) (NPs, in comparison with that of commercial powder for the methylene blue (MB) degradation under Ultra-Violet (UV) irradiation, showed the appropriate activity of nanostructures obtained by $Zn(NO_3)_2$ and $Zn(CH_3COO)_2$ precursors. The first-order kinetic constant over ZnO from $Zn(NO_3)_2$ was 1.9, 3.7 and 1.5 times of ZnO commercial powder, ZnO from $ZnCl_2$ and $Zn(CH_3COO)_2$, respectively. The ZnO NPs from $Zn(NO_3)_2$ and $Zn(CH_3COO)_2$ precursors have the best photocatalytic degradation performance with a degradation rate of 99.3% and 96.4%, respectively. It is found that the higher photocatalytic performance was probably due to the larger crystallinity, purity phase and specific morphologies than smaller particle size effect. A decrement in the crystallite size yields in a larger surface areas and enhances the adsorption of reactants and that paves the way to an enhancement in the photocatalytic performance. Thus, the synthetized ZnO is nanoparticles by the soft hydrothermal process which is a promising candidate for the photocatalytic purposes of dyes from waters.

1. Introduction

The organic pollutants are widely found in various industries, such as textile, paper, plastics, cosmetic, pharmaceutical and others. These pollutants seriously generate water pollution problem that may have harmful effects on the microorganisms living in several ecosystems. Because, in part, they prevent the sunlight penetration into water and reduce photosynthetic activity [1-3]. Most of the organic dyes are resistant to biodegradation under light. The direct photolysis of these colorant dyes in the naturel aquatic environment is thus hard [4]. The metal oxide semiconductors mediated photocatalysis reaction using the UV or visible light, under ambient conditions. It can harvest the

light energy and significantly enhance the rate of the dyes degradation [1, 5-7]. The photocatalysis is an eco-friendly method for environmental treatments to removal dyes in the wastewater that does not cause toxic by-products [6]. The organic pollutant molecules are break-down via an oxidative processes. There are several semiconductor materials that have shown great potential to, photocatalytically, degrade several molecules in water, such as TiO_2, ZnO, ZnS, SnO_2, WO_3 and CdS. [8-10]. TiO_2 is the most used effective photocatalyst, but it has been found that ZnO is an alternative photocatalyst material due to its photochemical stability, high efficiency, lower exciton recombination rate, greater surface area, high electronic mobility, non-toxic and abundant nature and low cost synthesis processes [6, 9]. It has been reported by Baruah et al. that ZnO has emerged as a more efficient photocatalyst than TiO_2 due to its high surface reactivity owing to its large number of active surface defect states [11]. Its high reaction and mineralization rates are due to its more efficient generation of hydroxyl ions.

Zinc oxide is a well known functional semiconductor, with unique physical and chemical properties. ZnO is a wide band gap of 3.37 eV and has large exciton binding energy (60 meV) at room temperature [12]. This compound is biosafe and biodegradable for the environment protection. The photocatalytic efficiency of ZnO can be improved through a number of ways; doping with metal and nonmetal elements, coupling with narrow bandgap materials, creating surface defects and specific morphologies, higher ratio of exposed ZnO polar facets or promotion the separation and transportation of the photo-excited charge carriers. [8, 9, 13-15]. Kumbhakar et al. have inspected the tuning of high defects states on ZnO nanostructures by a simple thermal annealing for the complete photo-degradation of MB dyes [9]. MacLaren et al. have demonstrated that the shape factor seems to be of overriding importance on the photocatalytic rate, reaching 5 times higher activity for some controlled morphology; Zn nanocrystals [16]. From the according to literature, the morphology and crystallites size of ZnO nanostructures can be tuned by controllable synthesis parameters and thermal heating conditions (precursor, solvent type, surfactants, reaction temperature and temperature calcination) in a particular synthesis technique [17, 18]. There is a reciprocity relationship between the cristanility size and the performance, namely the higher the size of cristanility is, the better the photocatalytic performance. Several reports have focused on the influence of different zinc salts type on the microstructure and the shape of ZnO nanostructures [17-23]. Shaba et al. reported that Zn precursors have little effect on the crystallite size of produced ZnO nanostructures but exerted greater influence on the morphology [18]. Depending on each parameters of the synthesis methods and their effects on the ZnO nanosystems crystallinity or morphology, there are still divergent views. The mechanisms of the ZnO nanostructures growth synthesis in correlation with the microstructural and morphological characteristics are not fully understood [18, 20]. Especially, the effect of precursors on the ZnO morphology for hydrothermal synthesis [20]. Consequently, the photocatalytic properties of ZnO oxide for the colorants degradation from water do not achieve maximum effectiveness. More investigations are still need to deploy for the optimization of all the synthesis parameters [18].

In this work, an investigation on the ZnO nanoparticles synthesis by varying the initial type salts (i.e., zinc acetate $Zn(CH_3COO)_2$, zinc nitrate $Zn(NO_3)_2$ and zinc chloride $ZnCl_2$) for the purpose of application of the final products as photocatalysts for methylene blue degradation as a model dye under UV irradiation. For a comparison of the photocatalytic behaviour of the prepared NPs, a nitrate commercial ZnO powder was taken. Mainly, the paper is so a contribution to the simple strategy synthesis of the functional zinc oxide catalyst as well as the investigation of the microstructural and morphological aspects.

2. Materials and Methods

$Zn(NO_3)_2$, $Zn(CH_3\ CO_2)_2$ and $ZnCl_2$ were used as zinc precursors to prepare ZnO nanoparticles through simple hydrothermal method. Hydrothermal synthesis method is attractive for several reasons: low cost, less hazardous and relatively low temperature operating [24]. Adequate quantities of slats, separately, were dissolved in 50 mL of distilled water and commercially NaOH for each solution with a magnetic stirring then transported into an autoclave. The powders were

washed several times to remove all the impurities and air-dried at room temperature. A heat treatment of the ZnO products was carried out at the temperature of 500°C for 12 hours.

The crystallinity of powders was investigated using X-ray diffraction (XRD) technique by PAN alytical X'pert Pro powder diffractometer with Cu-K_α radiation, (λ_{Cu} = 1.5418 Å). The morphology analysis was carried out in a Philips. XL 30 scanning electron microscope with a voltage of 30 kV. The optical characteristics of nanoparticles were studied using the diffuse reflectance spectroscopy on a Varian Cary 100 UV-Vis spectrophotometer with DRA-CA-30I.

The photocatalysis experiments were carried out using homemade photochemical reactor. The photocatalytic reactor consists of a Pyrex beaker settled on a magnetic agitator, which contains 50 ml of the colored aqueous solution. The MB pollutant concentration solution was 10 ppm, 250 mg/L of ZnO nanoparticles was added in a volume of 50 mL of the MB solution. A magnetic stirring in the dark for 5 minutes was sufficient to achieve the adsorption-desorption equilibrium. The used consisted irradiation system of an UVC lamp non-immersing; a Philips germicide (G15T8/15W) type, which mainly emits at 254 nm. The distance between the lamp and the beaker was fixed at 10 cm. The concentration was determined by measuring the absorbance (optical density) at λ = 664 nm of the MB solution for well-determined time intervals. After each 20 min, 3 ml of MB solution was analyzed by an UV-Visible spectrophotometer after centrifugation at 3000 rpm for 10 min, to follow the evolution of the absorbance spectra and the photocolorization of the BM. The solution was continuously stirred to ensure the uniform dispersion and de-agglomeration of the ZnO photocatalysts.

3. Results and Discussion

XRD analysis is an accurate asset to determine the crystal structure and crystallite size of a specimen. The XRD patterns of the ceramic powders are depicted in (Fig. 1). The diffraction patterns show sharp and well-defined diffraction peaks. The peak positions are found well matching with those of the standard pattern of ZnO hexagonal phase with a wurtzite structure phase according to (JCPDS card No. 36-1451). No impurity and other pics were observed reflecting the high purity of the synthesized ZnO NPs by using $Zn(CH_3COO)_2$ and $Zn(NO_3)_2$ precursors, except for the final product obtained with $ZnCl_2$ source material. According to (JCPDS card No. 07-0155) attributed to simonkolleite material, the incomplete reaction leads to the appearance of diffraction peaks relative to ($Zn_5(OH)_8Cl_2H_2O$) phase. The ZnO diffraction peaks on (Fig. 1) are narrow and exhibit an important intensity, which suggests that the nanoparticles zinc oxide have a good crystalline quality. The highest peaks are observed at 2θ = 36.39°, 36.37° and 36.42° for ZnO-acetate, ZnO-nitrate and Commercial ZnO are the characteristic crystalline peak of pure ZnO crystals that follow (101) plane reflection.

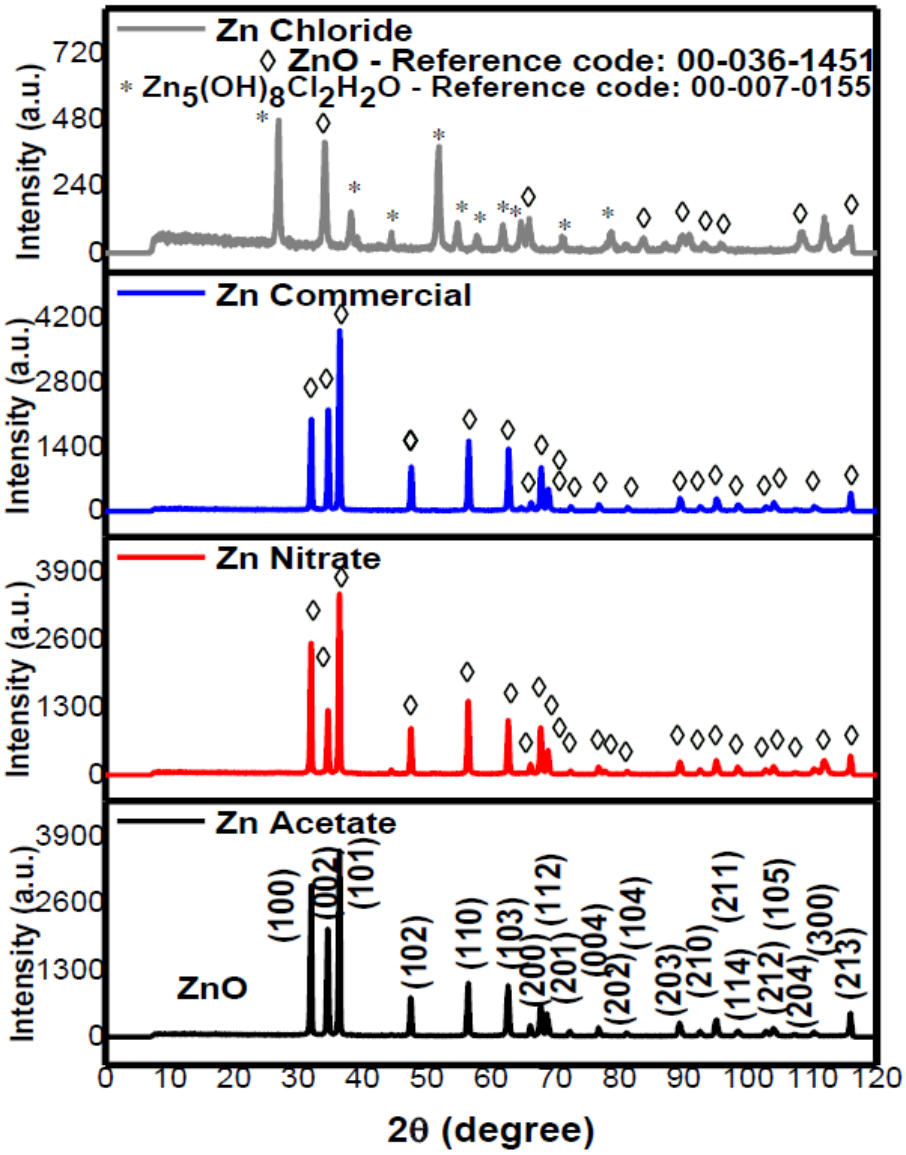

Fig. 1. XRD patterns of ZnO nanoparticles synthesized with zinc acetate, zinc nitrate, zinc chloride precursors and commercial powder.

In the ZnO hexagonal structure, the lattice constants '*a*' and '*c*' were calculated by using the equations (1) and (2) [25]:

$$d_{hkl} = \frac{1}{\sqrt{\frac{4(h^2+k^2+hk)}{3a^2}+\frac{l^2}{c^2}}} \quad (1)$$

$$n\lambda = 2d_{hkl}\sin\theta_{hkl} \quad (2)$$

Where d_{hkl} is the spacing between lattice planes of Miller indices (h, k and l) and n is the order of diffraction (usually n is equal to 1).
With the first-order approximation, $n = 1$;

$$\sin^2\theta = \frac{\lambda^2}{4a^2}\left[\frac{4}{3}(h^2+k^2+hk)+\left(\frac{a}{c}\right)^2 l^2\right] \quad (3)$$

The lattice constants a for (100) plane according to the Bragg equation is calculated by the Eq. 4 [26, 27]:

$$a = \frac{\lambda}{\sqrt{3}\sin\theta} \tag{4}$$

The lattice constant c for the plane (002) is given by the Eq. 5 [26, 27]:

$$c = \frac{\lambda}{\sin\theta} \tag{5}$$

Information on the crystallites size (D) for the sample was obtained from the full width at half maximum of the diffraction peaks using the Scherrer formula (6) [28, 29]:

$$D = \frac{0.94\lambda}{\beta_{(hkl)}\cos\theta_{(hkl)}} \tag{6}$$

where λ, $\theta_{(hkl)}$, and $\beta(hkl)$ are the X-ray wavelength (0.15418 nm), Bragg diffraction angle, and the full width in radians at half maximum intensity line, respectively.

From X-ray diffraction data, the crystallite sizes estimated using Scherrer equation (6) with the width of the most intense peak (101) plane for ZnO NPs fabricated using zinc acetate and zinc nitrate precursors are found to be 37 and 36 nm, respectively (see Table 1). The crystallite size calculated for ZnO nanoparticles synthesized from major diffraction plane (002) of zinc chloride precursor is 20 nm. The lattice constants of the ZnO structures are calculated and are in agreement with the reported values which are $a = b = 3.249$ Å and $c = 5.207$ Å according to the JCPDS data reflecting the high crystallinity of namely $Zn(CH_3COO)_2$ and $Zn(NO_3)_2$ precursors produced ZnO NPs. By varying zinc salts, the nano-size of ZnO particles do not greatly change, mainly with the use of $Zn(CH_3COO)_2$ and $Zn(NO_3)_2$ precursors via the same hydrothermal synthesis process. Shaba et al. have reported a conclusion [18], which is consistent with the obtained observations in this paper.

Table 1. The XRD data of the different precursors ZnO synthesized nanoparticles.

Salt precursor	Pos. [°2Th.]	FWHM [°2Th.]	Identified planes (h k l)		D, [nm]	*A,* [Å] *C,* [Å]
Zinc Acetate	36.387	0.234	101	ZnO	37.284	3.233 5.191
Zinc Nitrate	36.372	0.241	101	ZnO	36.264	3.233 5.188
Zinc Chloride	34.119	0.4337	002	ZnO	20.029	3.033 4.948
Zinc Commercial	36.419	0.2793	101	ZnO	31.293	3.230 5.177

The scanning electron micrographs of the synthesized samples with different magnifications are shown in (Fig. 2, 3).

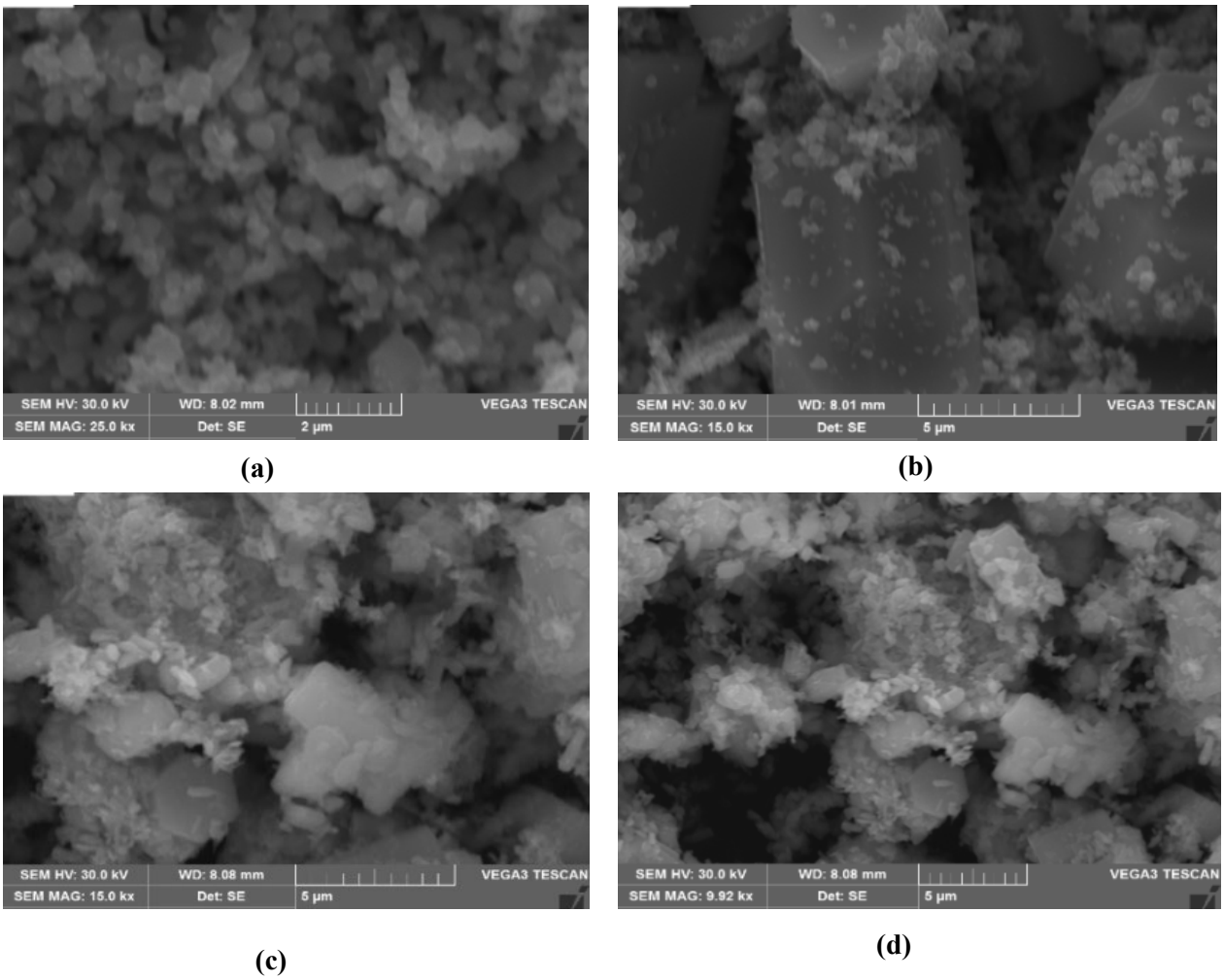

Fig. 2. SEM images of ZnO NPs obtained with (a-b) zinc acetate, (c-d) zinc nitrate

It is observed that the prepared ZnO-Acetate and ZnO-Nitrate in addition with Commercial-Nitrate powder form hexagonal rod-like structures. The shape of particles using ZnO-Chloride is spherical. The ZnO particles show massive nano- to micron-size aggregation [30]. Kaenphakdee et al. explain this extensive aggregation due to the particle requirements to reduce the surface energy and increase stability [30]. The particles of the ZnO-Acetate powder (Fig. 2a) have the uniform morphology-distribution and the high density than ZnO-Nitrate (Fig. 2b) and Commercial-Nitrate powder (Fig. 3d). The rods from commercial powder are irregular in form and randomly in distribution, the agglomerated particles exhibited pores resulting from escape of volatile substances or gases formed during calcination (Fig. 3c and Fig. 3d). However, the particles like branch-rod from using ZnO-Nitrate are smaller in dimension (Fig. 2c and Fig. 2d), there are some elongated structures in the form of rods with lengths in the order of 2 µm [31]. A large size of ZnO-Acetate rod approximately 5 µm in diameter and 6 µm length is expected (Fig. 2b). Interestingly, (Fig. 2a) shows formation of hexagonally prismatic structures [32, 33], these discs are observed to be stacked symmetrically in pairs in length. The pairs together apparently resemble layered hexagonal rods [33]. Natrchalayuth et al have found that the ZnO morphology of hexagonal prism crystals obtained from hydrothermal method using Zn acetate.

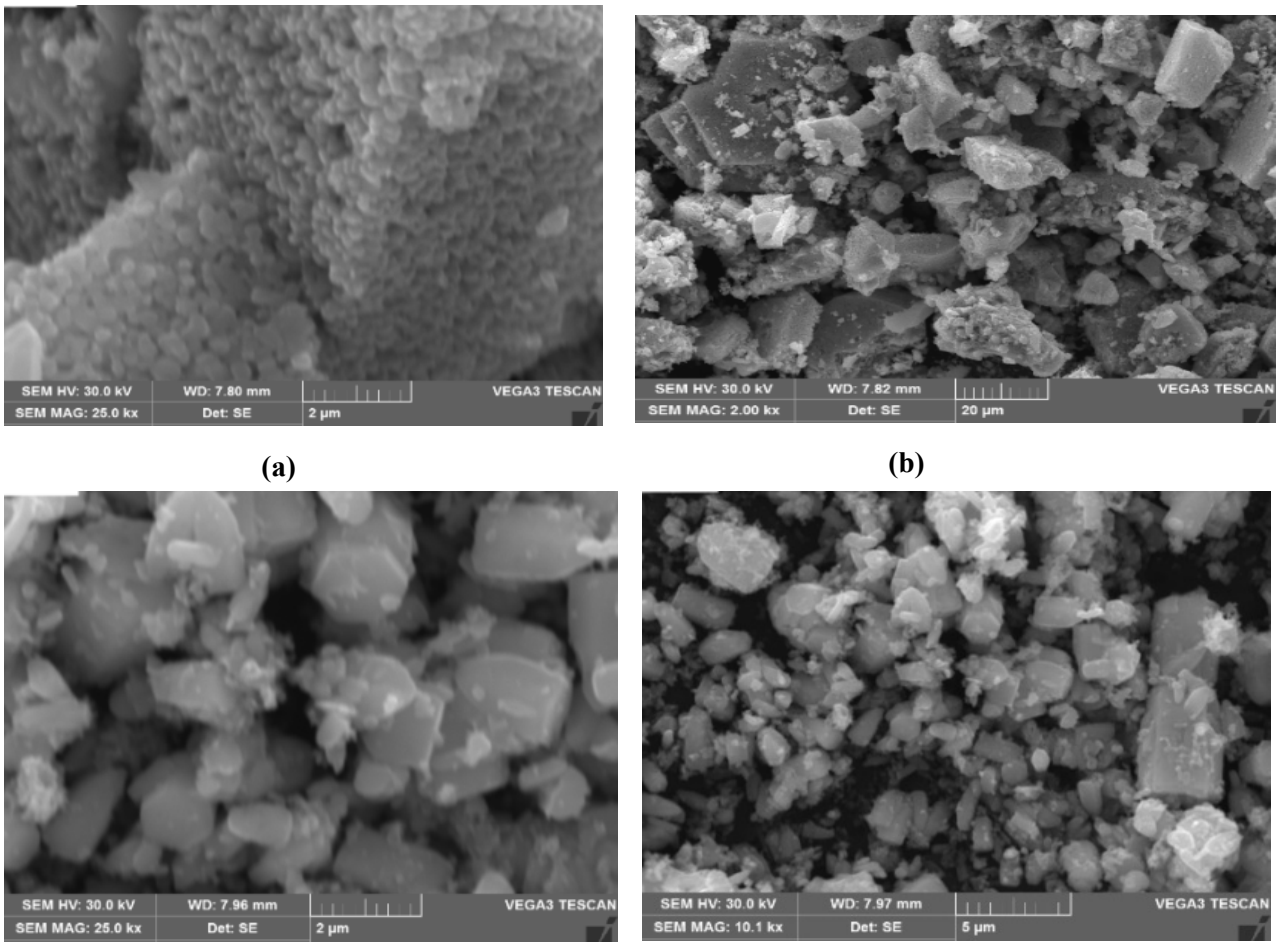

Fig. 3. SEM images of ZnO NPs obtained with (a-b) zinc chloride precursors and (c-d) commercial powder.

precursor was uniformly transformed to small spherical and rod like particles when pH solution was increased [32]. This can be described by the dissolution/re-precipitation mechanism under hydrothermal reaction [32]. With the increase of zinc acetate to Trizma (TB) mole ratio through hydrothermal process; Boppella and co-researchers established that the synthetized ZnO changed from irregular hexagonal prismatic structures to uniform hexagonal twin discs and finally into truncated hexagonal cones (3D trapezoids) [33]. Effect of using different precursors on the ZnO particles morphologies is observed [34, 35].

To inspect the optical absorption properties and bandgap energies of samples, UV-Vis diffuse reflectance spectra were measured. DRS is a more convenient technique for analyzing unsupported materials as UV-Vis absorption spectroscopy, because it takes advantage of the enhanced scattering phenomenon in powder materials and not require a powder sample to be dispersed in any liquid medium preventing its contamination [36]. The UV-Vis total reflectance of ZnO powders is presented in (Fig. 4a). It is observed that in the UV and visible regions, low and high reflectance were noted for all ZnO samples. As it is known, low reflectance corresponds to high absorbance. Thereby, all ZnO structures demonstrate barely reflection in the UV region due to their excellent absorption properties as it is reported by several researchers [30, 37, 38]. The relevant increase in the reflectance is related to the direct band gap of ZnO structure due to the transition of an electron from the valence band to the conduction band $\left(O_{2p} \rightarrow Zn_{3d}\right)$ [38]. The enhancing of the UV photons absorption and the excitation of electrons, can contribute to the improvement of the photocatalytic potential of materials. ZnO structures obtained from the use of zinc acetate and zinc nitrate displayed the lowest reflection in the visible range indicating their high

absorption also of the visible light. Thus, their suitable use as photocatalysts under UV and visible irradiations. The absorption edges of the different powders are very closely. A very slight blue shift is observed in the absorption edge for the synthetized ZnO nanostructures from zinc acetate and zinc nitrate as compared to those of zinc chloride precursors. This shift can be due to the enhancement of the crystallinity of zinc acetate and zinc nitrate based ZnO structures [39]. Other factors lead to the red or blue shift of ZnO nanocrystals like, changes in the morphologies, defect creation, band edge bending, crystallites size and surface microstructures [6, 37- 39]. Diffuse reflectance spectra of ZnO structures are shown in (Fig. 4b).

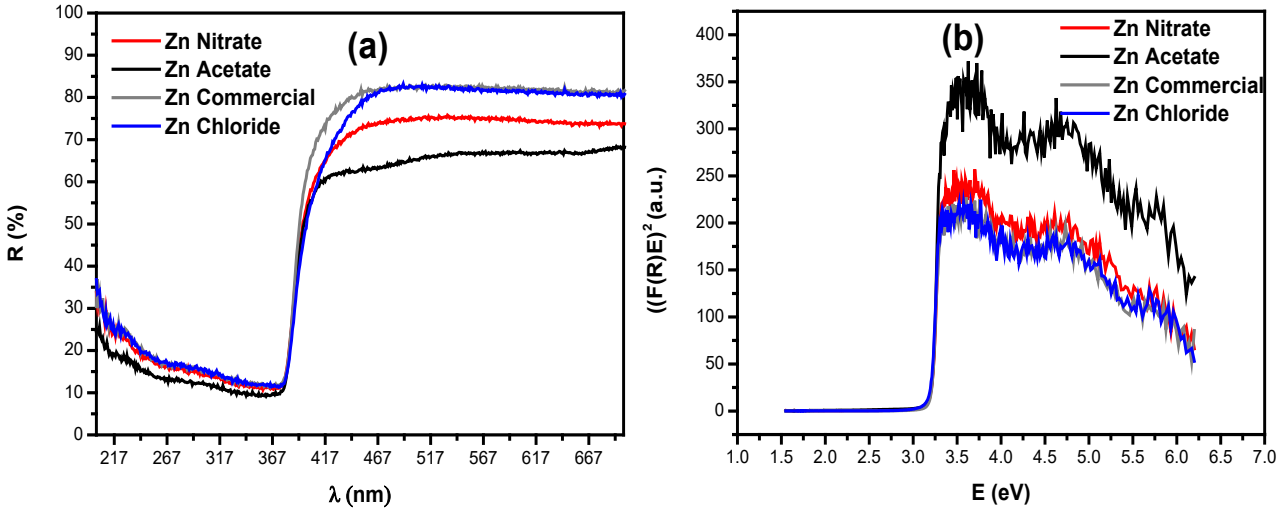

Fig. 4. (a) Total reflectance spectra of ZnO nanoparticles are prepared from different precursors and commercial ZnO powder and (b) $[F(R)E]^2$ against photon energy of ZnO nanostructures.

The Kubelka-Munk (K-M) function $F(R)$ was used to convert reflectance measurements into equivalent absorption spectra. Diffuse reflectance data were transformed according to the K-M model by the following relation [40, 41]:

$$F(R) = \frac{(1 - R_\infty)^2}{2R_\infty} = \frac{K}{S} \tag{7}$$

where, $R_\infty = {}^{R}/_{100}$ is the diffuse reflectance of the material and R is the reflectance; $F(R)$ is the Kubelka-Munk function, which corresponds to the absorbance and it was directly proportional to the absorption coefficient K, and inversely proportional to the scattering coefficient S. The absorption coefficient of a direct band gap semiconductor is related to Tauc's equation [42]:

$$\alpha h\upsilon = A\left(h\upsilon - E_g\right)^2 \tag{8}$$

where α is the linear absorption coefficient of the semiconductor, $h\upsilon$ is the photon energy, A is a constant. The E_g (the bandgap energies) values were thus estimated by extrapolation the linear portion of the function curve with the energy axis. The bandgap energies using K-M transformed reflectance spectra of the commercial ZnO and the synthetized powders from $Zn(NO_3)_2$, $ZnCl_2$ and $Zn(CH_3\ CO_2)_2$ were 3.21eV (Fig. 5d), 3.21eV (Fig. 5a), 3.21eV (Fig. 5c), and 3.22eV (Fig. 5b), respectively, which is consistent with the observed slight shift in the band-edge absorption and with the energies reported in the literature [36, 39]. The precursor material according to synthesis process, does not significantly affect the bandgap of the synthetized nanoparticles; Sheikhi et al. have found the same result for ZnO nanoparticles via the sol-gel method [43]. Thus, the present hydrothermal method produces ZnO nanostructures, which are in the blue region compared to the bulk ZnO (3.34 eV) [37].

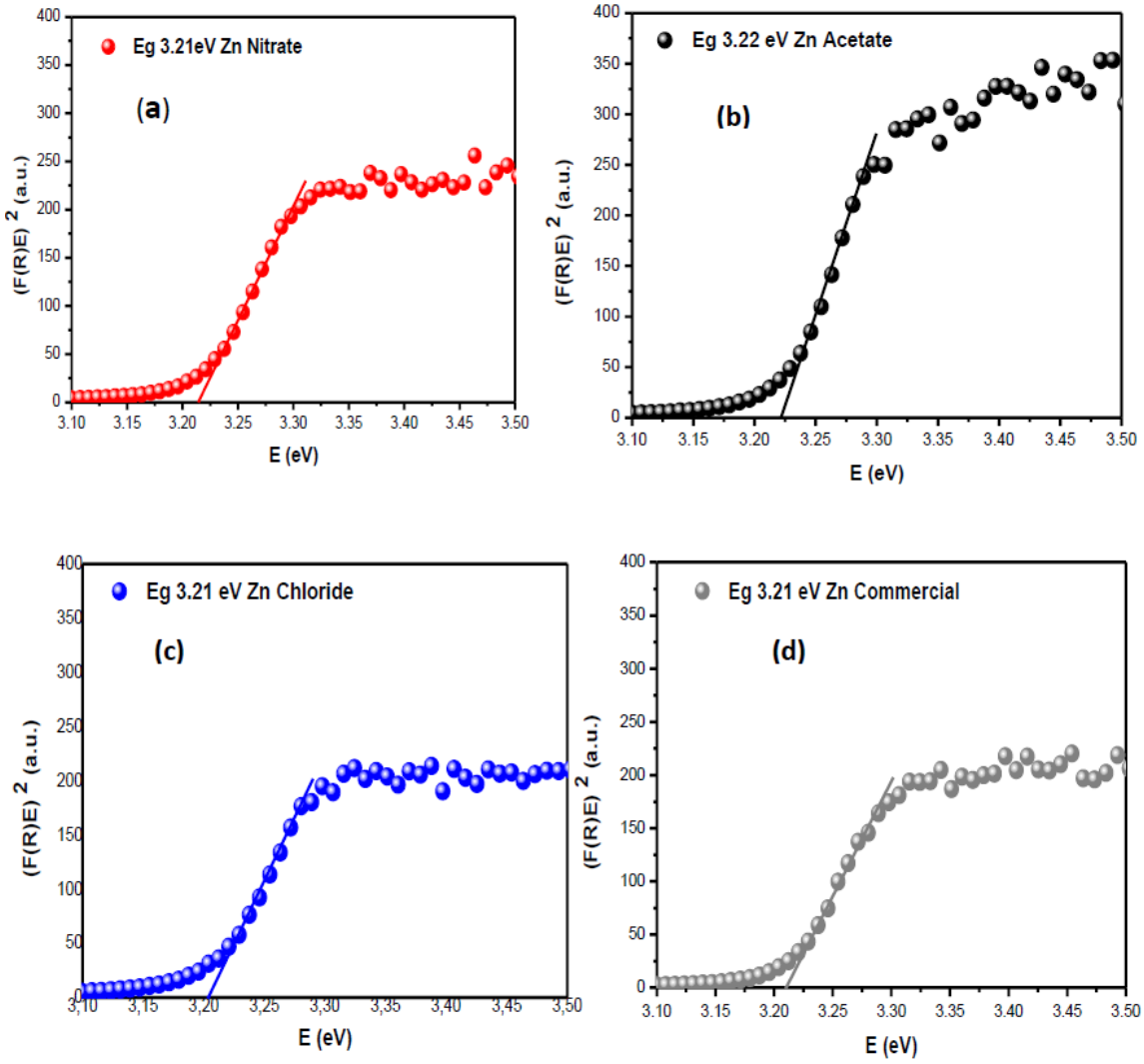

Fig. 5. Diffuse reflectance spectra (DRS) using Kubelka-Munk function of the ZnO commercial powder (d) and the synthetized ZnO NPs from $Zn(NO_3)_2$ (a), $ZnCl_2$ (c) and $Zn(CH_3\ CO_2)_2$ salts (b).

The photocatalytic activity of the synthetized ZnO nanoparticles from different precursors in comparison with commercial ZnO powder was evaluated by using (250 mg/L) catalyst for the degradation of MB (15ppm, 50 mL) under UV light source at ambient temperature and pH ~ 6.8-7.1 (Fig. 6A and Fig. 6D) show UV-visible spectral absorbance changes following the degradation of BM textile dye as a function of UV irradiations time using different synthetized and commercial ZnO nanoparticles catalysts. It is observed that the intensity of the principal characteristic absorption peak around ($\lambda_{max} = 664\ nm$) of the MB decreases with the increase in the time of irradiation under UV light. This indicates a break in the chromophore structure of the contaminant [31]. As seen from (Fig. 6A and Fig. 6D), the UV-visible spectra of MB under light irradiation have confirmed two absorption peaks at 664 nm and 612 nm which have been related to the monomer and dimer of MB [41]. All the two MB peaks were decreased in intensity reflecting the decolorization of the dye. Initially, there is a difference in their intensities, the absorption peak at $\lambda_{max} = 664\ nm$ is more higher than the one at $\lambda_{max} = 612\ nm$. In the presence of catalysts after 200 minutes, this difference was attenuated indicating that the rate of monomers degradation is much important than that of the dimers one. Thus, the most intense peak ($\lambda_{max} = 664\ nm$) was taken to follow the evolution of the MB degradation process and the calculations that will follow. From (Fig. 6D and Fig. 6C), it was noticed that MB dye was not completely degraded in 200 minutes by ZnO commercial powder and produced ZnO structures from $ZnCl_2$ source material under UV irradiations excitation. On the other hand, during the same interval time of 0 to 200

minutes, more MB degradation efficient with ZnO NPs generated by $Zn(NO_3)_2$ and $Zn(CH_3\ CO_2)_2$ precursors was noted, (see Fig. 6A and Fig. 6B).

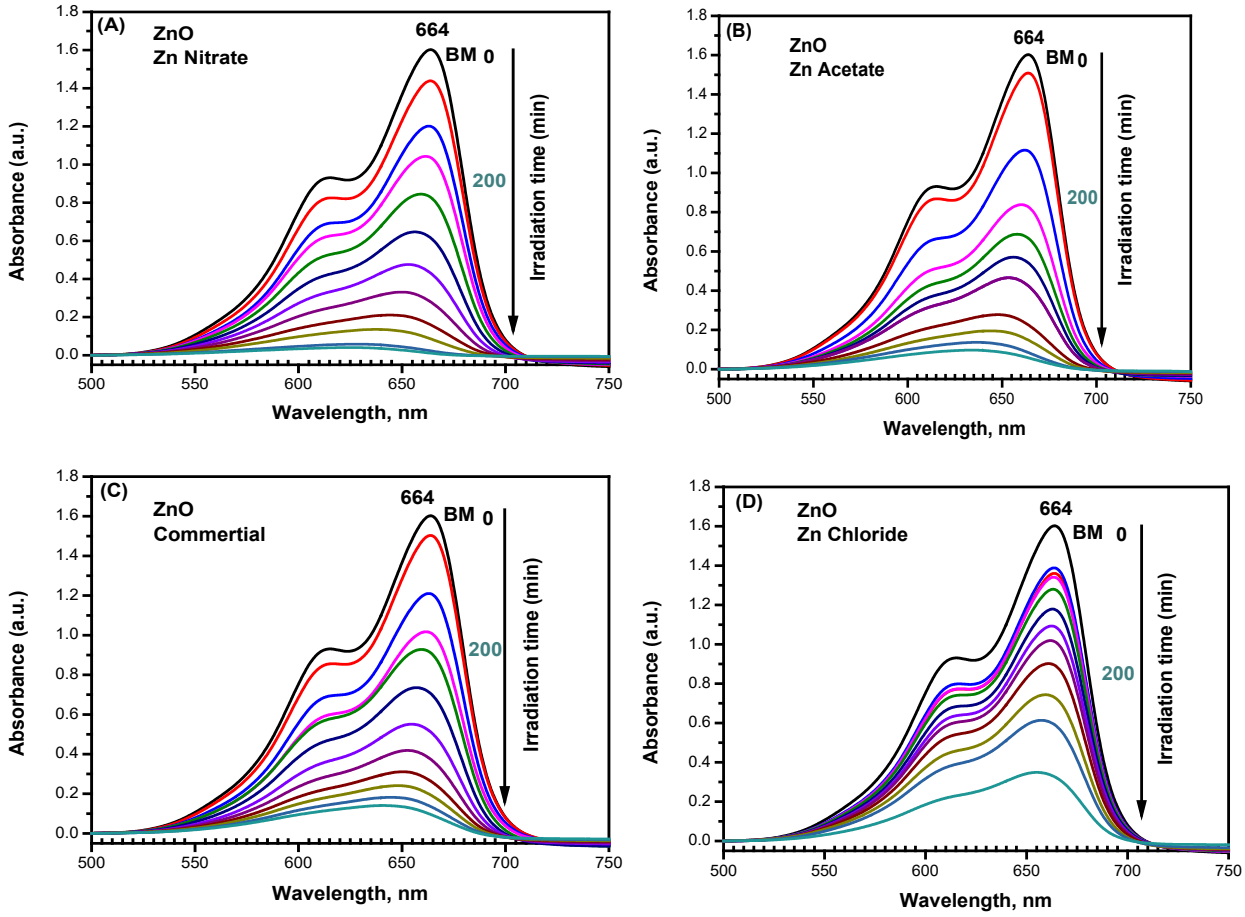

Fig. 6. UV-visible spectra evolution of the MB dye solution as a function of the UV irradiations times with the commercial powder and the different as-synthetized ZnO structures from: (A) $Zn(NO_3)_2$, (B) $Zn(CH_3\ CO_2)_2$, (C) commercial powder and (D) $ZnCl_2$ source material. Reaction condition: Dye concentration (10 ppm, 50 mL) with 250 mg/L of photocatalyst.

The degradation rate towards MB dye, after a time *t* of reaction, was calculated according to the following formula [44]:

$$\text{Degradation (\%)} = \frac{C_0 - \text{C}}{C_0} \times 100 \qquad (9)$$

Where C_0 is the initial concentration of the MB dye in the solution and C is the concentration after an irradiation time (*t*).

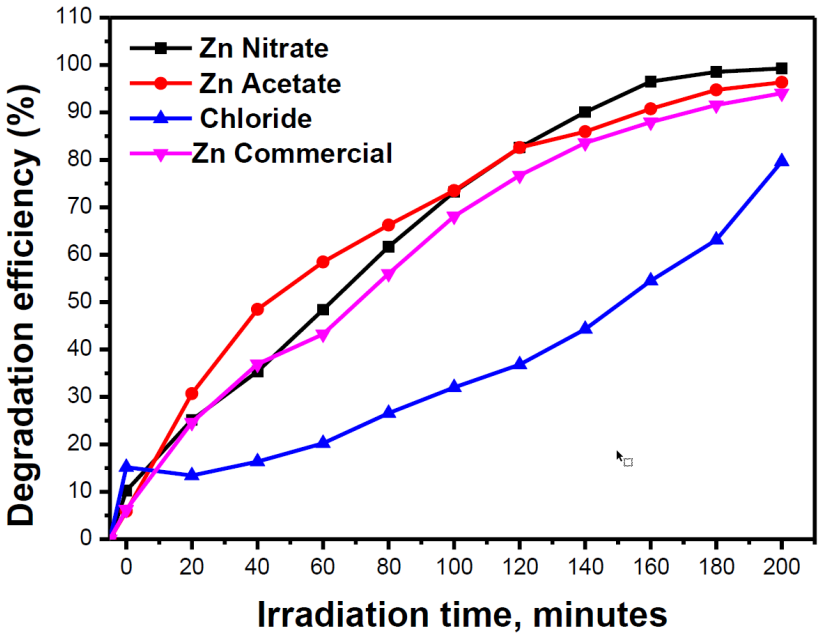

Fig. 7. Plot of the photocatalytic degradation efficiencies *vs.* times of methylene blue dye by synthetized and commercial ZnO photocatalysts.

To evaluate the efficiency of photocatalysts, the degradation rate was calculated. The variation of the degradation rates as function of the time of the irradiation of the different ZnO photocatalysts is illustrated in (Fig. 7).

As far as (Fig. 8), it reflects that the decolorization of MB was nearly completely degraded with the use of produced ZnO nanoparticles from $Zn(NO_3)_2$ and $Zn(CH_3\ CO_2)_2$ precursors and also ZnO commercial nanomaterial. The percentage of removal of MB dye, after 200 minutes, was about 99.31% and 96.38% for ZnO nanostructures synthetized by $Zn(NO_3)_2$ and $Zn(CH_3\ CO_2)_2$, respectively and 94.07% for commercial ZnO powder. While, the use of $ZnCl_2$ as zinc source material for the removal of MB pollutant is less efficient reaching the rate of 79.66% after the same time of reaction. These results display faster and higher MB decolorization under the UV irradiation through ZnO photocatalysts synthetized using $Zn(NO_3)_2$ and $Zn(CH_3\ CO_2)_2$ precursors. To understand the kinetics and estimate the pseudo-first-order constant of the MB photodegradation by ZnO nanoparticles, the plot of $ln\frac{C_0}{C}$ as function of time reaction was explored, (Fig. 8). The following law may express Langmuir-Hinshelwood model, valid for pollutants concentrations in the millimolar range [39, 45, 46]:

$$ln\frac{C_0}{C_t} = kt \tag{10}$$

where k is the constant rate of the photodegradation process which was estimated through the above the reaction equation (10).

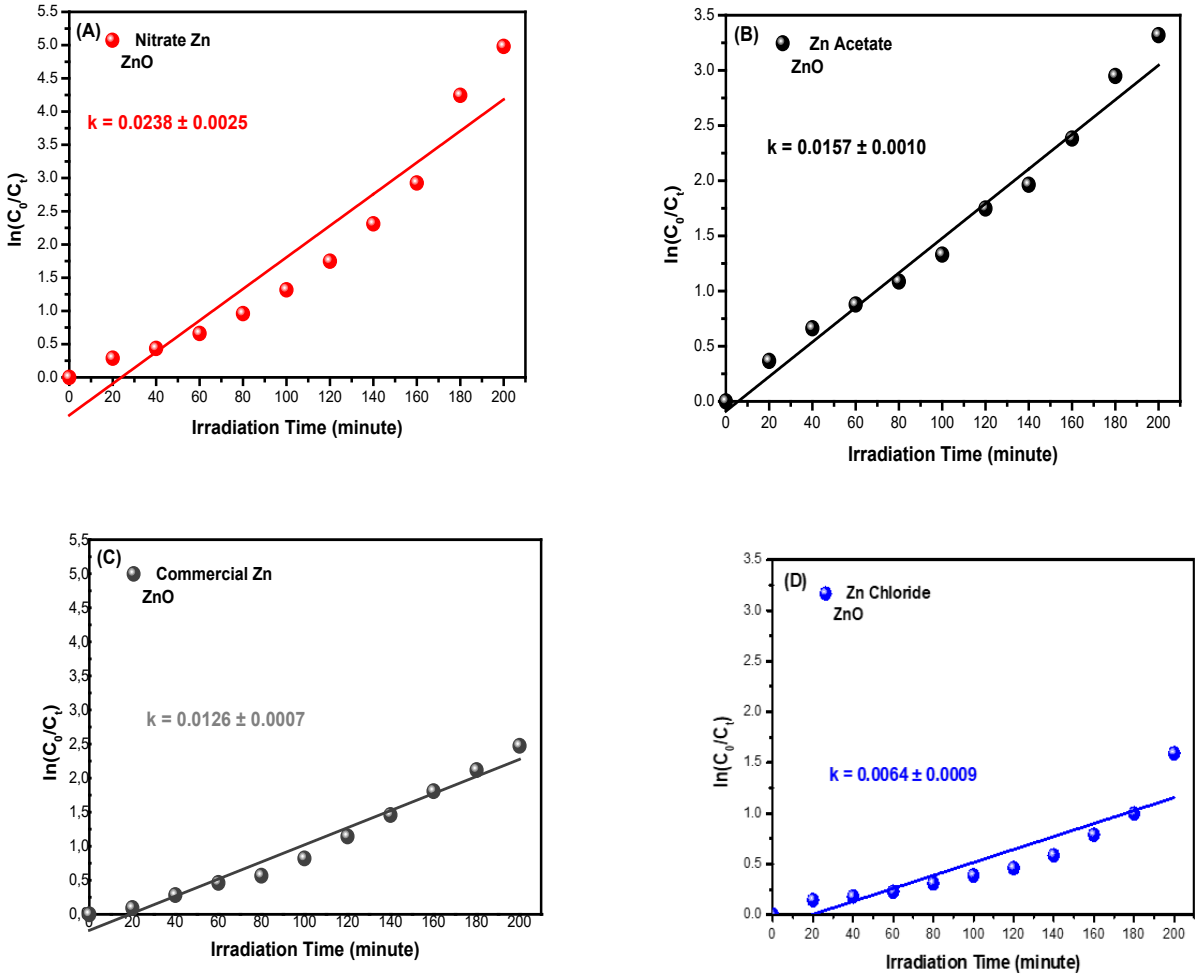

Fig. 8. Kinetic fits as function of the reaction times under the UV irradiation for the ZnO commercial nanoparticles and the different produced ZnO nanostructures using: (A) $Zn(NO_3)_2$, (B) $Zn(CH_3\ CO_2)_2$, (C) commercial powder and (D) $ZnCl_2$ as source material.

The curves of $ln(C_0/C_t)$ against reaction time (t) were nearly straight lines. The estimated k parameter values of the different samples; (slope of the plots), were 0.0238 min^{-1}, 0.0157 min^{-1}, 0.0126 min^{-1} and 0.0064 min^{-1} for ZnO_from $Zn(NO_3)_2$ salt, ZnO_from $Zn(CH_3\ CO_2)_2$ salt, commercial ZnO and ZnO_from $ZnCl_2$ salt, respectively. ZnO photocatalyst synthetized from $Zn(NO_3)_2$ salt has therefor exhibit the highest photodegradation k constant, followed by ZnO nanomaterial synthetized from $Zn(CH_3\ CO_2)_2$ precursor, commercial ZnO powder and the less efficient photocatalyst was ZnO nanoparticles synthetized from $ZnCl_2$ salt.

It is known that the photocatalytic activity efficiency of ZnO catalysts is influenced by their high specific surface area and small particle size, surface and bulk defects (oxygen vacancies), band gap energy, crystallinity and crystal facets, morphology-dependent charge transfer effects, specific porous morphologies and shapes, modification by sensitization through coupling with a narrow band gap material or by doping [39, 47-49]. Even though, the small crystallites which means high surface area can generate more active sites, fast mass transportation of the reactant and prolong light absorption edge [47], in this work small crystallites size (~ 20 nm of ZnO catalysts from $ZnCl_2$ precursor) do not govern the photocatalytic response since the nanoparticles exhibit poor photodegradation compared to the other samples. The poor photocatalytic activity of these catalysts may be due to the impurity ZnO phase and the presence of an amount of residual zinc oxide hydroxide hydrate phase. Jansanthea et al. report that the proportion and phase purity that inhibits the recombination of electron-hole pairs and the highest crystallinity are the most influential factors

enhancing the photocatalytic activity [45]. Ferreira et al. also observed that the porous ZnO nanostructures calcined at 700°C have the highest photocatalytic activity in spite of being the nanosystem with the lowest specific surface area due to the high crystallinity of these ZnO nanoparticles which is the most critical factor influencing the photocatalytic activity [39]. The authors explained that does crystallinity reflects a decrease in the relative concentration of bulk to surface defects which not only act as adsorption sites but also as charge carrier traps inhibiting the recombination of e^-/h^+ pairs [39]. According to Srinivasan et al., the spherical ZnO nanostructures possessed the highest specific surface area but exhibited the lowest photocatalytic activity among the other oriented nanorods, bicons and square bipyramids structures [50]. The researchers proposed that high crystallinity and mesoporous architecture are essential to the high photocatalytic activity [47, 50]. In this work, both produced ZnO nanostructures from $Zn(NO_3)_2$ and $Zn(CH_3\ CO_2)_2$ precursors as well as commercial ZnO powder exhibited excellent crystallinity which intervenes in part in a good photocatalytic response, namely for the two ZnO synthetized nanostructures (especially since they are characterized by practically similar sizes of crystallites 36 and 37 nm, respectively). Others factors affect the photocatalytic response of the samples. According to Shidpour et al. the photocatalytic activity of ZnO nanocrystals is not only sensitive to crystal size but also to morphology [51]. Imran Din et al. reported that the photocatalytic activity efficiency of the ZnO catalysts is also dependent on the structural and morphological aspects [52]. Generally, porous ZnO nanostructures can lead to high photocatalytic activity [47]. This is due to; they have strong adsorption capability, an efficient electron-hole separation and promoted the diffusion and mass transportation of dye molecules [47]. According to the MEB observations (Fig. 2, 3) and MB photo-degradation results (Fig. 7), the produced ZnO nanoparticles by zinc acetate salt have a more are faster than kinetics in the half time reaction de-colorization than the ZnO nanoparticles produced against zinc nitrate salt, but this status was reversed in the second half time. This may be due to the higher density of the ZnO nanostructures from $Zn(CH_3\ CO_2)_2$ which limits the dye penetration and adsorption, the saturation of the active sites adsorption is attained. It is observed that the commercial ZnO powder is also porous but there is a non-ordered porosity and the grains distribution is not homogenous, so the photo-response was limited, comparatively to the ZnO catalysts generated from $Zn(NO_3)_2$ and $Zn(CH_3\ CO_2)_2$ precursors. By correlating the different observations together, a conclusive evidence that the crystallites size was not only the factor that affects the organic dye photo-degradation response as reported in the literature [33, 53]. Additionally, In [54], researcher conducted a research on a multistage hydrothermal technique which was established to synthesize hierarchical zinc oxide with a high surface to volume ratios paving the way to producing a low cost, large scale and low temperature of ZnO. In [55], the authors studied the different preparation methods of ZnO–graphene composites, they elaborately analyzed the fundamentals and usefulness of characterization techniques, then they have experimentally carried out the influence of ZnO's morphology in photocatalytic behavior of the composites.

The crystallinity, (i.e. crystal state, phase purity and composition) and the morphology aspects such as particles shape and pores size and distribution affect the photocatalytic activity efficiency of the ZnO nanoparticles catalysts under UV irradiations with the MB as pollutant dye model. It is noteworthy to say the morphology, size and chemical properties of nanoparticles are classified based on the physical and chemical characteristics', some of the well-known classes of NPs are given in [56]. In [57], Zinc oxide (ZnO) nanoparticles (NPs) were synthesized by applying the Rosmarimus officinalis leaf extract at 80°C (ZnO-80) and 180°C (ZnO-180), they found that the size of NPs of ZnO-80 was remarkably smaller than that of ZnO-180 which forms flakier agglomerated spherical-like structures. Noticeably, the temperature in this work is constant comparatively to [57], in which the temperature was taken with different values.

Furthermore, the extremely small size of nonaparticles and their large surface area render them appropriate candidate for a wide range of applications.

4. Conclusion

In this paper, a reliable method called hydrothermal synthesis process has been performed using different zinc materials for the sake of producing ZnO functional nanoparticles as well as studying its effect on structural and morphological, optic, and mythelene blue photocatalytic. The verification process of NPs was experimentally carried out based on XRD, SEM, UV-Vis, and DRS. To emphasize, the estimated crystallites size was in the range of 20-37 nm. Nanoparticles based on $Zn(NO_3)_2$ and $Zn(CH_3\ CO_2)_2$ perfectly synthesized by an excellent crystanility in addition to the commercial ZnO powder P25. The produced nanosystem using $ZnCl_2$ metal salt was a fog-like (mist) of zinc oxide and zinc chloride hydroxide hydrate phases. The band gap energies of the nanoparticles are analytically calculated using the reflectance spectra by means of the Kubelka-Munk function. Additionally, the optical band gap energies energies were approximately 3.21, 3.21, 3.21 and 3.22 eV for the commercial ZnO and the synthetized powders from $Zn(NO_3)_2$, $ZnCl_2$ and $Zn(CH_3\ CO_2)_2$, respectively. Interestingly, the precursor type does not affect the E_g when it comes to the identical conditions of the present hydrothermal synthesis method. From a structural point of view, different morphologies of the produced ZnO nanostructures were obtained with the variation of the zinc precursor. Using $Zn(CH_3COO)_2$ and $Zn(NO_3)_2$ precursors. The shape of ZnO and $ZnCl_2$ was rod-like and spherical-like morphologies, respectively.

The photocatalytic activity of the prepared ZnO NPs compared to the nitrate commercial powder; it is noticed a degradation in the level of methylene blue (MB) dye under the UV illumination. Furthermore, the synthetized pure ZnO NPs using soft hydrothermal method, zinc nitrate and zinc acetate precursors yield the best photocatalytic activities for MB degradation under UV light irradiation. The first-order kinetic constant over ZnO NPs from $Zn(NO_3)_2$ (0.02376 min^{-1}) was 1.9, 3.7 and 1.5 times of ZnO commercial powder (0.01255 min^{-1}), ZnO NPs from $ZnCl_2$ (0.0064 min^{-1}) and ZnO NPs from $Zn(CH_3COO)_2$ (0.01568 min^{-1}), respectively. Noticeably, ZnO NPs from $Zn(NO_3)_2$ and $Zn(CH_3COO)_2$ precursors provide with the best photocatalytic degradation performance with a decrease rate of 99.3% and 96.4% after 200 min of reaction, respectively. The higher photocatalytic response was probably due to larger crystallinity and purity phase and also their specific morphologies than smaller particle size effect.

References

[1] V-E. Podasca and M-D. Damaceanu, Photopolymerized Films with ZnO and Doped ZnO Particles Used as Efficient Photocatalysts in Malachite Green Dye Decomposition, Appl. Sci. 10:6 (2020) 1954; Doi.10.3390/app10061954.

[2] P-A. Luque-Morales, A. Lopez-Peraza, O-J. Nava-Olivas, G. Amaya-Parra, Y-A. Baez-Lopez, V-M. Orozco-Carmona, H. Garrafa-Galvez and M-J. Chinchillas-Chinchillas, ZnO Semiconductor Nanoparticles and Their Application in Photocatalytic Degradation of Various Organic Dyes, Mat. 14 (2021) 7537; https://doi.org/10.3390/ma14247537.

[3] M. Naidu Subramaniam, P. Sean Goh, W. Jye Lau and A. Fauzi Ismail, Review The Roles of Nanomaterials in Conventional and Emerging Technologies for Heavy Metal Removal: A State-of-the-Art Review, Nanomaterials, 9 : 4 (2019) 625; doi:10.3390/nano9040625.

[4] M. Movahedi, A. Hosseinian, M. Bakhshaei, M. Rahimi and I. Arshadnia, Micro-spherical SnO_2/Zn_2SnO_4: Synthesis, heat treatment and photocatalytic efficiency for decolorization of two dye mixture in wastewater, Journal of Applied Chemistry, 11 : 41 (2017).

[5] H. Wanga, L. Zhanga, C. Junqing, H. Shijie, L. Zhaohui Wanga, J. Liua and X. Wang, Semiconductor heterojunction photocatalysts, design, construction, and photocatalytic performances, Tutorial Review, Chem. Soc. Rev. (2014); DOI.10.1039/c4cs00126e.

[6] H. Khuder Naji, A. Mirza Oda, W. Abdulaljeleel, H. Abdilkadhim, and R. Hefdhi, ZnO-Ag/PS and ZnO/PS Films for Photocatalytic Degradation of Methylene Blue, Indones. J. Chem. 20: 2 (2020) 314 – 323; DOI: 10.22146/ijc.41347.

[7] F. Fresno, R. Portela, S. Su´arezc and J. M. Coronado, Photocatalytic materials, recent achievements and near future trends, J. Mater. Chem. A. 2 (2014) 2863; DOI. 10.1039/c3ta13793g.

[8] T. Bora and J. Dutta, Applications of Nanotechnology in Wastewater Treatment A Review, J. Nanosci. Nanotechnol. 14 : 1 (2014) 613–626; doi:10.1166/jnn.2014.8898.

[9] P. Kumbhakar, S. Biswas, P. Kumbhakar, Observation of high photocatalytic activity by tuning of defects in chemically synthesized ethylene glycol capped ZnO nanorods, Optik. 154 (2018) 303–314; https://doi.org/10.1016/j.ijleo.2017.10.039.

[10] Chandrappa K. Govindappa, Venkatesha T. Venkatarangaiah, Sharifah B. Abd Hamid1, Electrochemical Generation of Cubic Shaped Nano Zn2SnO4 Photocatalysts, Nano-Micro Lett,5(2). 101-110 (2013)/ http://dx.doi.org/10.5101/nml.v5i2.p101-110

[11] S. Baruah, M. Jaisai, R. Imani, M. Nazhad and J. Dutta, Photocatalytic paper using zinc oxide Nanorods, Sci. Technol. Adv. Mater. 11 (2010) 7; doi. 10.1088/1468-6996/11/5/055002.

[12] Y. Zhang, M.K. Ram, E.K. Stefanakos, and D. Yogi Goswami, Review Article Synthesis, Characterization, and Applications of ZnO Nanowires, Journal of Nanomaterials. (2012) 22; doi.10.1155/2012/624520.

[13] A. Omo Ibhadon and P. Fitzpatrick, Review Heterogeneous Photocatalysis, Recent Advances and Application, Catalysts. 3 (2013)189-218; Doi.10.3390/catal3010189.

[14] F. Kayaci, S. Vempati, I. Donmez, N. Biyikli, T. Uyar, Role of zinc interstitials and oxygen vacancies of ZnO in photocatalysis: a bottom-up approach to control defect density, Nanoscale. 6 (2014) 10224–10234.

[15] L Gang, J. C. Yu., Q. L. Gao and C. Hui-Ming, Crystal Facet Engineering of Semiconductor Photocatalysts: Motivations, Advances and Unique Properties, Chem, Commun. 47 (2011) 6763−6783.

[16] A. Mclaren, T.;Valdes-Solis, G. Li, S.C. Tsang, Shape and size effects of ZnO nanocrystals on photocatalytic activity. J. Am. Chem. Soc. 131 (2009) 12540–12541; DOI: 10.1021/ja9052703.

[17] E. Kwabena Droepenu, B. Siong Wee, S. Fun Chin, K. Ying Kok, M. Firdaus Maligan, Zinc Oxide Nanoparticles Synthesis Methods and its Effect on Morphology, A Review, Biointerface Research in Applied Chemistry. 12: 3 (2022) 4261–4292; DOI. 10.33263/BRIAC123.42614292.

[18] E. Y. Shaba, J. O. Jacob, J. O. Tijani and M. A. T. Suleiman1, A critical review of synthesis parameters afecting the properties of zinc oxide nanoparticle and its application in wastewater treatment, Applied Water Science.11:48 (2021); https://doi.org/10.10Q7/s13201-021-01370-z.

[19] J. Mayekar, V. Dhar, S. Radha, Role of Salt Precursor in the Synthesis of Zinc Oxide Nanoparticles, IJRET: International Journal of Research in Engineering and Technology. 03 (2014); eISSN: 2319-1163 | pISSN: 2321-7308.

[20] E. Özel, I. Gözde Tuncolu, C. Asçiksari, E. Suvaci, Effect of Precursor Type on Zinc Oxide Formation and Morphology Development during Hydrothermal Synthesis, Hittite Journal of Science and Engineering. 3:2 (2016) 73-80; DOI.10.17350/HJSE19030000034. ISSN Number: 2149-2123.

[21] N. Srinivasa Rao, M. V. Basaveswara Rao, Structural and Optical Investigation of ZnO Nanopowders Synthesized from Zinc Chloride and Zinc Nitrate, American Journal of Materials Science. 5:3 (2015) 66-68; DOI: 10.5923/j.materials.20150503.02.

[22] T. Saidani, M. Zaabat, M. S. Aida, R. Barille, M. Rasheed and Y. Almohamed, Influence of precursor source on sol–gel deposited ZnO thin films Properties, J Mater. Sci: Mater. Electron. 28 (2017) 9252–9257; DOI 10.1007/s10854-017-6660-9.

[23] N. Lehraki, M.S. Aida, S. Abed, N. Attaf and M.Poulain, ZnO thin films deposition by spray pyrolysis: Influence of precursor solution properties, Current Applied Physics. (2012); doi:10.1016/j.cap.2012.03.012.

[24] S. Dhara and P. K. Giri, ZnO Nanowire Heterostructures: Intriguing Photophysics and Emerging Applications, Rev. Nanosci. Nanotechnol. 2:3 (2013) 1–24; doi:10.1166/rnn.2013.1032.

[25] M.F. Malek, M.H. Mamat, M.Z. Musa, Z. Khusaimi, M.Z. Sahdan, A.B. Suriani, A. Ishak, I. Saurdi, S.A. Rahman and M. Rusop, Thermal annealing-induced formation of ZnO nanoparticles: Minimum strain and stress ameliorate preferred c-axis orientation and crystal-growth properties, J. All. Comp. 610 (2014) 575–588.

[26] P. Bindu and S. Thomas, Estimation of lattice strain in ZnO nanoparticles: X-ray peak profile analysis, J. Theor Appl. Phys. 8 (2014) 123–134; DOI 10.1007/s40094-014-0141-9.

[27] E. Solati and D. Dorranian, Estimation of lattice strain in ZnO nanoparticles produced by laser ablation at different temperatures, J. of Appl. Spectr. 84:3 (2017); DOI 10.1007/s10812-017-0497-0.

[28] A. Abdalla, S. Bereznev, N. Spalatu, O. Volobujeva, N. Sleptsuk, M. Danilson, P. laser deposition of Zn(O, Se) layers in nitrogen background Pressure. 9:17443 (2019).

[29] S. Iaiche, C. Boukaous, D. Alamarguy, A- Djelloul and D. Hamana, Effect of Solution Concentration on ZnO/$ZnAl_2O_4$ Nanocomposite Thin Films Formation Deposited by Ultrasonic Spray Pyrolysis on Glass and Si(111) Substrates, J. of Nano Resea. 63(2020) 10-30.

[30] S. Kaenphakdee, P. Putthithanas, S. Yodyingyong, J. Leelawattanachai, W. Triampo, N. Sanpo, J. Jitputti and D. Triampo, Zinc Oxide Synthesis from Extreme Ratios of Zinc Acetate and Zinc Nitrate: Synergistic Morphology, Mater. 15:570 (2022); https://doi.org/10.3390/ma15020570.

[31] E.C. da Silva, M.O.S. de Moraes, W.R. Brito, R.R. Passos, R.F. Brambilla, L.P. da Costa and L.A. Pocrifka, Synthesis of ZnO Nanoparticles by the Sol-Gel Protein Route: A Viable and Efficient Method for Photocatalytic Degradation of Methylene Blue and Ibuprofen, J. Braz. Chem. Soc. 31:8 (2020) 1648-1653.

[32] K. Natrchalayuth, T. Wasanapiarnpong, S. Larpkiattaworn, P. Sujaridworakun, Hydrothermal Synthesis of Zinc Oxide Nanoparticle from Zinc-Dust Waste for Photocatalytic and Antibacterial Applications, Advanced Materials Research. 506 (2012) 78-81; Doi.10.4028/www.scientific.net/ AMR.506.78.

[33] R. Boppella, K. Anjaneyulu, P. Basak, and Sunkara V. Manorama, Facile Synthesis of Face Oriented ZnO Crystals, Tunable Polar Facets and Shape Induced Enhanced Photocatalytic Performance, dx.doi.org/10.1021/jp311443s | J. Phys. Chem. C. 117 (2013) 4597−4605.

[34] M. Gusattia, G.S. Barroso, C.E. Maduro de Campos, D. Aragão Ribeiro de Souza, J. de Almeida do Rosário, R. Bohn Lima, C. Cardoso Milioli , L. Abreu Silva, H. Gracher Riella, N. Cabral Kuhnen, Effect of Different Precursors in the Chemical Synthesis of ZnO Nanocrystals, Materials Research. 14:2 (2011) 264-267; DOI: 10.1590/S1516-14392011005000035.

[35] Z. Kovács, C. Molnár, T. Gyulavári, K. Magyari, Z-R. Tóth, L. Baia, Z. Pap, K. Hernádi, Solvothermal synthesis of ZnO spheres: Tuning the structure and morphology from nano- to micro-meter range and its impact on their photocatalytic activity, Catalysis Today. 397-399 (2022) 16–27; https://doi.org/10.1016/j.cattod.2022.03.004.

[36] A. Escobedo Morales, E. Sánchez Mora and U. Pal, Use of diffuse reflectance spectroscopy for optical characterization of un-supported nanostructures, Revista Mexicana De Física S. 53:5 (2007) 18–22.

[37] D. Papadaki, G.H. Mhlongo, D.E. Motaung, S.S. Nkosi, K. Panagiotaki, E. Christaki, M.N. Assimakopoulos, V.C. Papadimitriou, F. Rosei, G. Kiriakidis, and S.S. Ray, Hierarchically Porous Cu‐ Co‐ and Mn-Doped Platelet-Like ZnO Nanostructures and Their Photocatalytic Performance for Indoor Air Quality Control, ACS Omega. 4 (2019) 16429−16440; http://pubs.acs.org/journal/ acsodf.

[38] A. Khorsand Zak, A. Manaf Hashim and M. Darroudi, Optical properties of ZnO/$BaCO_3$ nanocomposites in UV and visible regions, Nanoscale Research Letters. 9 (2014) 399; http://www.nanoscalereslett.com/content/9/1/399.

[39] S. Henriques Ferreira, M. Morais, D. Nunes, M. João Oliveira, A. Rovisco, A. Pimentel, H. Águas, E. Fortunato and R. Martins, High UV and Sunlight Photocatalytic Performance of Porous ZnO Nanostructures Synthesized by a Facile and Fast Microwave Hydrothermal Method, Materials. 14 (2021) 2385; https://doi.org/10.3390/ma14092385 https://www.mdpi.com/journal/materials.

[40] K. Kara, E. Şenadim Tüzemen, R. Esen, Annealing effects of ZnO thin films on p-Si(100) substrate deposited by PFCVAD, Turk. J. Phys. 38 (2014) 238-244; doi:10.3906/_z-1310-3.

[41] E. Prabakaran and K. Pillay, Synthesis of N-doped ZnO nanoparticles with cabbage morphology as a catalyst for the efficient photocatalytic degradation of methylene blue under UV and visible light, RSC Adv. 9 (2019) 7509; DOI: 10.1039/c8ra09962f.

[42] K.G. Chandrappa, T.V. Venkatesha, Electrochemical Synthesis and Photocatalytic Property of Zinc Oxide Nanoparticles, Nano-Micro. Lett. 4:1 (2012) 14-24; http://dx.doi.org/10.3786/nml.v4i1. p14-24.

[43] S. Sheikhi, M. Aliannezhadia, F. Shariatmadar Tehrani, Effect of precursor material, pH, and aging on ZnO nanoparticles synthesized by one-step sol–gel method for photodynamic and photocatalytic applications, Eur. Phys. J. Plus. 137:60 (2022); https://doi.org/10.1140/epjp/s13360-021-02252-8.

[44] K. Shanmugam Ranjith, A. Senthamizhan, B. Balusamya and T. Uyar, Nanograined surface shell wall controlled ZnO–ZnS core–shell nanofibers and their shell wall thickness dependent visible photocatalytic properties, The Royal Society of Chemistry Catal. Sci. Technol. (2017).

[45] P. Jansanthea, J. Kanthabangharn, W. Chomkitichai, J. Ketwaraporn, C. Saovakon, C. Wansao, A. Wanaek, P. Kraivuttinun, P. Pookmanee, S. Phanichphantt, Temperature-controlled synthesis and photocatalytic properties of ZnO–SnO_2 nanocomposites, J. Aust. Ceram. Soc. 57 (2021) 579–588; https://doi.org/10.1007/s41779-021-00567-4.

[46] A. Isai Kalpesh, S. Shrivastava Vinod, Photocatalytic degradation of methylene blue using ZnO and 2% Fe-ZnO semiconductor nanomaterials synthesized by sol-gel method: A comparative study. J. Water Environ. Nanotechnol. 4:3 (2019) 251-262; DOI. 10.22090/jwent.2019.03.008.

[47] Y. Sun, L. Chen, Y. Bao, Y. Zhang, J. Wang, M. Fu, J. Wu and D. Ye, The Applications of Morphology Controlled ZnO in Catalysis, Review, Catalysts. 6 (2016) 188; Doi.10.3390/catal6120188.

[48] M. Naidu Subramaniam, P. Sean Goh, W. Jye Lau and A. Fauzi Ismail, The Roles of Nanomaterials in Conventional and Emerging Technologies for Heavy Metal Removal: A State-of-the-Art Review, Nanomaterials. 9 (2019) 625; Doi.10.3390/nano9040625.

[49] M. Ali Johar, R. Arslan Afzal, A. Ali Alazba, and U. Manzoor, Review Article Photocatalysis and Bandgap Engineering Using ZnO Nanocomposites, Advances in Materials Science and Engineering. (2015) 22; http://dx.doi.org/10.1155/2015/934587.

[50] P. Srinivasan, B. Subramanian, Y. Djaoued, J. Robichaud, T. Sharma, R. Bruning, Facile synthesis of mesoporous nanocrystalline ZnO bipyramids and spheres: Characterization, and photocatalytic activity. Mater. Chem. Phys. (2015) 155 162–170.

[51] R. Shidpour, A. Simchi, Faegheh Ghanbari, M. Vossoughi, Photo-degradation of organic dye by zinc oxide nanosystems with special defect structure: Effect of the morphology and annealing temperature, Applied Catalysis A: General. 472 (2014) 198–204; http://dx.doi.org/10.1016/j.apcata.2013.12.003.

[52] M. Imran Din, J. Najeeb and G. Ahmad, Recent advancements in the architecting schemes of Zinc oxide based photocatalytic assemblies, Separation & Purification Reviews. (2017); DOI: 10.1080/15422119.2017.1383918.

[53] A.S. Cherevan, L. Deilmann, T. Weller, D. Eder and R. Marschall, Mesoporous Semiconductors, A New Model to Assess Accessible Surface Area and Increased Photocatalytic Activity, ACS Applied Energy Materials. 1:11 (2018) 5787-5799; https://pubs.acs.org/doi/10.1021/acsaem.8b01123.

[54] M. R. Alenezi, A. M. Almeshal, and A. N. Alkhaledi, “Hierarchical ZnO Nanomaterials with Superior Photocatalytic Properties,” in Journal of Nano Research, 2022, vol. 75, 59–70

[55] E. Albiter, A. S. Merlano, E. Rojas, J. M. Barrera-Andrade, Á. Salazar, and M. A. Valenzuela, “Synthesis, characterization, and photocatalytic performance of ZnO--graphene nanocomposites: a review,” J. Compos. Sci., vol. 5, no. 1, p. 4, (2020); DOI: 10.3390/jcs5010004

[56] I. Khan, K. Saeed, and I. d. Khan. "Nanoparticles: Properties, applications and toxicities." Arabian journal of chemistry 12.7 (2019): 908-931.

[57] Al-Garni, T.; A.Y. Abduh, N.; Al-Kahtani, A.; Aouissi, A. Synthesis of ZnO Nanoparticles by Using *Rosmarinus officinalis* Extract and Their Application for Methylene Bleu and Crystal Violet Dyes Degradation under Sunlight Irradiation. *Preprints* 2021, 2021040038 (doi: 10.20944/preprints202104.0038.v1)